Materials Today Bio 26 (2024) 101057

Contents lists available at ScienceDirect

Materials Today Bio

journal homepage: www.journals.elsevier.com/materials-today-bio

In situ administration of STING-activating hyaluronic acid conjugate primes anti-glioblastoma immune response

Teenesha Chellen [a], Mathilde Bausart [a], Pierre Maus [b], Kevin Vanvarenberg [a], Nisha Limaye [b], Véronique Préat [a,**], Alessio Malfanti [a,c,*]

[a] UCLouvain, Louvain Drug Research Institute, Advanced Drug Delivery and Biomaterials, Avenue Mounier 73 B1.73.12, 1200, Brussels, Belgium
[b] UCLouvain, de Duve Institute, Genetics of Autoimmune Diseases and Cancer, Brussels, Belgium
[c] Department of Pharmaceutical and Pharmacological Sciences, University of Padova, Via F. Marzolo 5, 35131 Padova, Italy

ARTICLE INFO

Keywords:
Glioblastoma
STING
Immunotherapy
Polymer-drug conjugates
Hyaluronic acid
MSA2

ABSTRACT

Glioblastoma (GBM) is an aggressive brain tumor, with a highly immunosuppressive tumor immune microenvironment (TIME). In this work, we investigated the use of the STimulator of INterferon Genes (STING) pathway as an effective means to remodel the GBM TIME through the recruitment of both innate and adaptive immune cell populations. Using hyaluronic acid (HA), we developed a novel polymer-drug conjugate of a non-nucleotide STING agonist (MSA2), called HA-MSA2 for the *in situ* treatment of GBM. In JAWSII cells, HA-MSA2 exerted a greater increase of STING signaling and upregulation of STING-related downstream cyto-/chemokines in immune cells than the free drug. HA-MSA2 also elicited cancer cell-intrinsic immunostimulatory gene expression and promoted immunogenic cell death of GBM cells. In the SB28 GBM model, local delivery of HA-MSA2 induced a delay in tumor growth and a significant extension of survival. The analysis of the TIME showed a profound shift in the GBM immune landscape after HA-MSA2 treatment, with higher infiltration by innate and adaptive immune cells including dendritic, natural killer (NK) and CD8 T cell populations. The therapeutic potential of this novel polymer conjugate warrants further investigation, particularly with other chemo-immunotherapeutics or cancer vaccines as a promising combinatorial therapeutic approach.

1. Introduction

Glioblastoma (GBM) is the most common and aggressive brain cancer, associated with poor prognosis [1,2]. The World Health Organization (WHO) established GBM as a grade 4 glioma, comprising up to 50 % of all gliomas [3]. GBM is currently an unmet clinical need due to its high recurrence after standard treatment (Stupp protocol), including surgery to remove the main tumor followed by concomitant radiation and adjuvant temozolomide chemotherapy to target residual tumor cells [4–6]. The 35–40 % of GBM patients who cannot be treated by surgery have an even worse prognosis. The median overall survival of patients with GBM is still low (8–15 months), and the current multimodal treatment strategy has only slightly improved median survival [7]. The failure of clinical and experimental therapeutic approaches is attributable to GBM cells that are endowed with numerous mechanisms of resistance related to location (e.g., the presence of the Blood Brain Barrier, BBB) [8], downregulation in the expression of potential therapeutic targets [9], and intra/inter-patient heterogeneity [10]. The number of therapeutics approved for GBM is very limited [11], and a combination of advances in drug discovery and drug delivery will be necessary to properly address these challenges.

Immunotherapies hold great promise for cancer treatment. However, current immunotherapeutic agents administered in monotherapy have failed to provide clinical benefits to patients with GBM [12,13]. Indeed, despite the success of immune checkpoint inhibitors (ICIs, e.g. anti-PD-1, anti-CTLA-4) in several tumors such as melanoma or lung cancers, these antibodies have not provided positive clinical outcomes in GBM as evidenced by the failure of recent phase III clinical trials with anti-PD-1 therapy [14,15]. The negligible immune response of GBM could be attributed to its "cold" immunological profile and immunosuppressive Tumor Immune Microenvironment (TIME): a low mutational burden and significant lack of tumor antigen-specific CD8 T cells,

* Corresponding author. UCLouvain, Louvain Drug Research Institute, Advanced Drug Delivery and Biomaterials, Avenue Mounier 73 B1.73.12, 1200, Brussels, Belgium. Department of Pharmaceutical and Pharmacological Sciences, University of Padova, Via F. Marzolo 5, 35131 Padova, Italy
** Corresponding author.
E-mail addresses: veronique.preat@uclouvain.be (V. Préat), alessio.malfanti@uclouvain.be, alessio.malfanti@unipd.it (A. Malfanti).

https://doi.org/10.1016/j.mtbio.2024.101057
Received 7 February 2024; Received in revised form 4 April 2024; Accepted 10 April 2024
Available online 16 April 2024

with myriad immune-suppressive cells such as Regulatory T cells (Tregs), Myeloid-Derived Suppressor Cells (MDSC) and M2-like tumor-associated macrophages and microglia (TAMs) in the highly immune-resistant TIME [12,16]. Therefore, new therapeutic targets are required to overcome the current limitations of GBM immunotherapy.

Recently, STimulator of INterferon Genes (STING) has been identified as a potential "druggable" immunotherapeutic target for cancer treatment [17–19]. STING is an endoplasmic reticulum-associated homodimer protein and the receptor for 2′,3′-cyclic guanosine monophosphate–adenosine monophosphate (cGAMP) [20]. Unlike other targets, STING is constitutively expressed in both cancer and immune cells at variable levels [21]. Activation of STING signaling induces the expression of type I interferon (IFN I) and pro-inflammatory cytokines, promoting the mobilization of antigen-presenting cells (APCs, e.g., dendritic cells (DCs) [22], macrophages [23] and microglia [24], critical responders to STING agonists), to prime CD8 T cells and in turn, to increase the tumor immunogenicity and to modulate the TIME [25,26]. It has been demonstrated that hyper-activation of STING signaling can induce cell death in cancer cells [27–29]; this increases the interest of harnessing this class of drugs that may not only re-shape the TIME but also exert a direct cytotoxic effect on cancer cells. Despite their potential, there has been little progress in the use of STING agonists for the immunotherapy of GBM [30,31]. Indeed, commonly used STING agonists, e.g., cyclic dinucleotides (CDNs) such as ADU-S100, suffer from low cell uptake and poor pharmacokinetic properties that limit their therapeutic use [32–34]. Current strategies exploited to trigger the STING pathway include the encapsulation of STING agonists into drug delivery systems [35,36], repurposing chemotherapeutics (e.g., platinum complexes [37,38]), or using metal-organic frameworks nanoparticles [39].

Recently, a novel non-cyclic nucleotide STING agonist called MSA2 has been developed, showing to stimulate innate immunity markers such as IFNβ. This STING agonist triggered a potent anticancer response in several "hot" preclinical tumor-bearing mouse models; however, the effects of MSA2 on the GBM TIME have not been explored in depth [40–43].

In this work, we hypothesized that *in situ* delivery of MSA2 could convert the immune-poor GBM TIME to a more immunogenic and inflamed ("hot") phenotype. To overcome its poor water solubility and enhance its delivery into the tumor, we designed a hyaluronic acid (HA)-drug conjugate optimized for the intracellular delivery of MSA2. We hypothesized that the conjugation of MSA2 to HA could trigger the effect of MSA2 thanks to i) the enhanced delivery via CD44 expressed on both GBM- and immune cells, ii) tunable linking chemistry that allows drug release into the cells [44], and iii) drainage into the brain lymphatic system (through binding of Lymphatic Vessel Endothelial hyaluronan receptor 1, LYVE-1, on lymphatic endothelial cells), modulating immune surveillance and response [45–49]. In addition, HA displays interesting immunomodulatory properties related to its interaction with Toll-Like Receptors (TLR)-2 and −4 on immune cells, activating a signaling cascade that promotes the release of immunostimulatory cytokines [50,51].

Previously, our group developed the first polymer-drug combination conjugates conceived for local chemo-immunotherapy of GBM: HA-conjugates carrying CpG and Doxorubicin, which combine an adjuvant that can activate innate immunity with an immunogenic cell death (ICD)-inducer that promotes adaptive immunity [52,53]. *In vivo* proof-of-concept of anti-GBM synergism has been achieved in the orthotopic GL261 model, with superior infiltration of CD8 T cells. Leveraging our experience in the use of HA for local treatment of GBM, we hypothesized that the conjugation of MSA2 to HA could provide an "all-in-one" immunotherapeutic agent, capable to impact the GBM immunity cycle by eliciting both innate and adaptive immune responses. Consequent to this design, we observed a superior activation of the STING pathway and an upregulation of type I IFN signaling in both immune and GBM cells mediated by HA-MSA2 over the free drug counterpart. Moreover, we showed that HA-MSA2 conjugate acts directly on GBM cells by inducing immunogenic cell death. Finally, the activity of the novel HA-MSA2 has been evaluated in a highly immunosuppressive orthotopic SB28 GBM model [54] demonstrating an extension of the survival and capacity to revert the "cold" GBM into "hot" showing a simultaneous activation of both innate and adaptative immune responses. To the best of our knowledge, our results provide the first evidence that *in situ* administration of STING-activating HA conjugate may be an effective immunotherapeutic modality for GBM, supporting further development of this approach.

2. Materials and methods

2.1. Materials and reagents

Hyaluronic acid (HA, 100 kDa) was purchased from Lifecore Biomedical, LLC (Chaska, MN, USA); 5,6-Dimethoxy-γ-oxobenzo [*b*]thiophene-2-butanoic acid (here referred as MSA-2) was purchased from MedChemExpress (HY-136927, South Brunswick, NJ, USA); 4-(4,6-dimethoxy-1,3,5-triazin-2-yl)-4-methylmorpholinium chloride (DMTMM Cl) was purchased from Sigma−Aldrich (St. Louis, MO, USA); ethylenediaminetetraacetic acid (EDTA) and TRIzol™ reagents were purchased from Thermo Fisher Scientific (Waltham, MA, USA); bovine serum albumin (BSA) were purchased from VWR International Srl (Leuven, Belgium); endotoxin-free TE buffer was purchased from Qiagen (Hilden, Germany). GoScript™ Reverse Transcription Mix and Oligo (dT) GoTaq® qPCR Master Mix were purchased from Promega (Madison, WI, USA). Oligonucleotide primers were purchased from Integrated DNA Technologies (IDT) (Leuven, Belgium) and are listed in supplementary information (SI) (table S1). The antibodies used and the relevant provider and dilutions are listed in SI. Unless otherwise specified, all reagents were purchased from Sigma−Aldrich (St. Louis, MO, USA).

2.2. Cell lines

Murine dendritic JAWSII cells (ATCC, Manassas, VA, USA) were maintained in MEM α, nucleosides, with no ascorbic acid, 1 mM sodium pyruvate and 5 ng/ml GM-CSF Recombinant Mouse Protein cultured at 37 °C in a 5 % CO_2 atmosphere. Murine macrophages J774 cells (ATCC, Manassas, VA, USA) were cultured in Dulbecco's modified Eagle's medium GlutaMAX with 4.5 g/L D-glucose without sodium pyruvate at 37 °C in a 5 % CO_2 atmosphere. Murine microglial BV-2 cells (American Type Culture Collection (ATCC), Manassas, VA, USA) were grown in Dulbecco's modified Eagle's medium GlutaMAX with 4.5 g/L D-glucose without sodium pyruvate at 37 °C in a 5 % CO_2 atmosphere. Murine glioma SB28 cells and murine GL261 cells (DSMZ, German Collection of Microorganisms and Cell Cultures GmbH, Leibniz Institute, Braunschweig, Germany) were cultured in Dulbecco's modified Eagle's medium (DMEM) with L-glutamine, 4.5 g/L D-glucose, and 1 mM sodium pyruvate at 37 °C in a 10 % CO_2 atmosphere. All the mediums were supplemented with 10 % fetal bovine serum (FBS) and 1.0 % antibiotics (penicillin/streptomycin).

2.3. Synthesis and characterization of hyaluronic acid (HA)-MSA2 conjugate

2.3.1. Synthesis of HA-MSA2

HA (200 mg, 0.496 mmol, 1 eq.) was dissolved in 20 mL of ultrapure water. After HA dissolution, DMTMM Cl (10.93 mg, 0.039 mmol, 0.08 eq.) was added to the solution, and the mixture was stirred at RT for 2 h. Next, the hydrazine derivative linker (0.06 eq.) was added to the mixture. The reaction was stirred at RT for 96 h and poured into 200 mL of cold ethanol (99 %) to obtain the HA-hydrazide (HA-Hz) derivative. The final product was collected and desiccated under a vacuum without further purification. HA-Hz (140 mg, 1 eq.) was dissolved in 20 mL of MilliQ water. After total conjugate dissolution, MSA2 (0.14 eq. in 1 mL

DMSO) was added to the mixture and the pH of the solution was decreased to 5 by adding acetic acid. The mixture was stirred for 72 h at 50 °C and poured into 200 mL of cold ethanol (99 %) to obtain the HA-MSA2 derivative. The final product was collected and desiccated under a vacuum. The conjugate has been characterized by 1H NMR and UV–Vis analysis. Yield: 92 mg (%w/w: 65 %).

^{1}H NMR (D_2O): δ ppm 7.54-7.40 (2H, b), 7.19-7.04 (1H, b), 4.53-4.30 (1H, bm), 4.02-2.97 (18H, bm), 2.08-1.74 (3H, s).

2.3.2. MSA2 loading

The drug loading of HA-MSA2 conjugate was determined by UV–VIS. The conjugate was dissolved in PBS, pH 7.4, and the absorbance of MSA2 was quantified at 324 nm. The absorbance of free HA was used as a blank. The drug content was calculated using MSA2 calibration curve ($\lambda = 324$ nm, 1–30 μg/mL, $R^2 = 0.99$).

2.3.3. Size and zeta potential

Dynamic light scattering (DLS) and zeta potential analyses were performed at 25 °C using a Malvern Zetasizer NanoZS system (Malvern Instruments Ltd., UK.). HA-MSA2 was dissolved in PBS, pH 7.4 (2 mg/mL), and was analyzed at a fixed angle of 173° at 25 °C with a red laser ($\lambda = 633$ nm). The zeta potential was measured by dissolving HA-MSA2 (2 mg/mL) in KCl (1 mM). All measurements were performed in triplicate.

2.4. In vitro studies

2.4.1. Western Blot analysis

JAWSII (murine dendritic) or SB28 (murine GBM) cells (10^6 cells/well) were seeded in 6-well plates and treated with 20 μM MSA2, HA or HA-MSA2 (drug equivalent concentration) for 0.5, 5 and 24 h. Untreated cells were used as controls. Cells were detached with TrypLE Express (Gibco, 12605-10) and lysed in 200 μL of lysis buffer (50 μM Tris-HCl, 150 μM NaCl, 2 μM EDTA, Nonidet P40 Substitute 0.01x (ThermoFisher, J19628), phosSTOP (Roche, 04906837001) and cOmplete (Roche, 11873580001)). 20 μL of each lysate was loaded onto 4–15 % gradient 10-well acrylamide gels (BioRad, 4561084), migrated by electrophoresis, transferred onto PVDF membranes, blocked 1h in 2 % milk (or 5 % BSA for pIRF3) in 1X TBS-Tween 0.1 % and then incubated overnight at 4 °C in primary antibody. Membranes were washed 3 × 5min in 1X TBS-Tween 0.1 %, incubated 1h in secondary antibody (HRP-coupled mouse anti-rabbit IgG; Cell Signaling, 7074) diluted 1/10 000 in 2 % milk in 1X TBS-Tween 0.1 %, washed 3 × 5min in 1X TBS-Tween 0.1 %, 1 × 5min in 1X TBS, and revealed using SuperSignal West Pico PLUS (Thermo, 3480) or SuperSignal West Femto (Thermo, 34095). Blots were visualized on a Fusion Solo S (Vilber Lourmat).

The following primary antibodies were used: Alpha-actinin at 1/1000 (Cell Signaling, 6487); GAPDH at 1/1000 (Cell Signaling, 2118); STING at 1/1000 (Cell Signaling, 13647); pSTING at 1/500 (Cell Signaling, 72971); TBK1 at 1/500 (Cell Signaling, 3504); pTBK1 at 1/500 (Cell Signaling, 5483); IRF3 at 1/500 (Cell Signaling, 4302); pIRF3 at 1/500 (Cell Signaling, 4947).

2.4.2. Quantitative real-time PCR (qPCR)

Immune cells (JAWSII J774 or BV-2) or GBM cells (SB28 or GL261) (2×10^5 cell/well) were seeded in 24-well plates. Cells were treated with 20 μM MSA2, HA or HA-MSA2 (drug equivalent concentration) for 5 and 24 h. Cells without any treatment were used as control. mRNA isolation was performed as follows: 200 μL of TRIzol™ and 40 μL of chloroform were added to each sample. Cells were centrifuged at 12 000 g × 15 min at 4 °C. mRNA was isolated by precipitation in a mixture of isopropanol and 75 % ethanol and re-dissolved in 10 μL of endotoxin-free TE buffer; the total mRNA concentration (ng/mL) and purity were assessed using a Nanodrop 2000 spectrophotometer (Thermo Scientific, USA). mRNA (0.33 μg/μL in TE buffer) was reverse transcribed using GoScript™ Reverse Transcription Mix, Oligo (dT) (Promega, USA). qPCR was performed using GoTaq® qPCR Master Mix (primer sequences are reported in table S1). Relative expression analysis was normalized against RPL19 or Actinβ as reference genes, and the relative level of expression was calculated using the comparative ($2^{-\Delta\Delta CT}$) method.

2.4.3. Cell viability assay

SB28 cells (5×10^3 cells/well), were seeded in 96-well plates. After 24 h, the cells were treated with free MSA2 or HA-MSA2 conjugate, in the range of 0.0001–20 μM MSA2 equivalent concentration. After 24 or 72 h, cells were fixed with paraformaldehyde (PFA, 4 % v/v in water) for 20 min and then were treated with 50 μL of crystal violet stain and incubated at room temperature for 30 min. The stain was washed three times with water and the plates were left to dry overnight. Finally, cells were treated with a solubilization solution of methanol, and the crystal violet absorbance (λ: 560 nm) was read with the SpectraMax ID5 microplate reader (Molecular Devices; San Jose, CA, USA). Data were normalized with the untreated group (100 % viability). IC50 values were calculated using a non-linear regression (curve-fit) mode.

2.5. Immunogenic cell death studies

2.5.1. Extracellular ATP detection assay

SB28 cells (2×10^5 cells/well) were seeded in a 12-well plate and maintained in a complete growth medium. The cells were treated with MSA2 or HA-MSA2 conjugate at 20 μM, equivalent MSA2 concentrations. After 24 h of incubation, the supernatant was collected, and the secreted level of extracellular ATP was measured with the real-time Glo ATP marker (Promega, Madison, WI, USA) according to the manufacturer's instructions using a Spectramax iD5 reader.

2.5.2. Calreticulin cell-surface flow cytometry

SB28 cells (2×10^5 cells/well) were seeded in 12-well plates and incubated for 24 h. Cells were treated with 20 μM, free MSA2 or an equivalent drug concentration of HA-MSA2. Following 24 h, cells were harvested with trypsin, washed three times with PBS and re-suspended in PBS supplemented with 5 mg/mL BSA and 100 μL of EDTA (0.5 M). Cells were transferred to a FACS 96-V-well plate for flow cytometry analysis and stained with the cell viability dye zombie aqua (Biolegend, San Diego, CA, USA) (dilution of 1:100) for 15 min at RT. Next, cells were stained with a primary anti-CLR antibody (rabbit anti-calreticulin monoclonal antibody; Invitrogen, Cambridge, UK) for 30 min at 4 °C protected from the light and then with a secondary APC-coupled antibody (goat anti-rabbit IgG H&L (APC); Abcam, Cambridge, UK) for 30 min at 4 °C in the dark and analyzed via flow cytometry using FACSVerse system (BD Bioscience, Franklin Lakes, NJ, USA) and analyzed using FlowJo software (FlowJo, Ashland, OR, USA).

2.5.3. Immune cells maturation assay

SB28 were seeded in a T25 plate (2×10^6 cells/plate) and maintained in a complete growth medium for 24 h. Next, cells were treated with 20 μM of free MSA2 or an equivalent drug concentration of HA-MSA2 for 72 h. In parallel, immune cells (JAWSII, J774 and BV-2, 1×10^5 cells/well) were seeded in a 24-well plate and cultured for 24 h at 37 °C. The conditioned media of pre-treated SB28 cells was incubated with the immune cells for 24 h. Following the time, cells were harvested and the maturation markers were obtained by staining immune cells with a primary APC/Cy7 anti-CD86 antibody (Biolegend, San Diego, CA, USA) for 30 min at 4 °C protected from the light, washed and analyzed through flow cytometry as discussed above.

2.6. In vivo studies

All experiments were performed following the Belgian national regulation guidelines and following EU Directive 2010/63/EU and were approved by the ethical committee for animal care of the Faculty of Medicine of the Université catholique de Louvain (2019/UCL/MD/004).

2.6.1. SB28 orthotopic GBM model

Immunocompetent six-week-old female C57BL/6J mice (Charles River Laboratories, Wilmington, MA, USA) were anesthetized by intraperitoneal injection of ketamine/xylazine (100 and 13 mg/kg, respectively). Next, mice were orthotopically grafted with 5×10^3 cells/mouse by convection-enhanced delivery (CED) using a Hamilton syringe (26S gauge needle) mounted on an infusion syringe pump on a stereotaxic frame (Harvard Apparatus, Holliston, MA, USA) at a rate of 0.5 μL/min. The following injection coordinates were used: i) 2.1 mm lateral, 0.5 mm posterior from the bregma, and ii) 2.6 mm deep from the outer border of the cranium [13].

2.6.2. In vivo imaging

Mice grafted with SB28 tumors were monitored by IVIS Spectrum In Vivo Imaging System on Days 7, 11, and 14. Mice were injected with Luciferin (i.p. injection of 50 μg/mL, 100 μL) 15 min before each analysis and the bioluminescence signal associated to the tumor growth has been registered.

2.6.3. In vivo anticancer activity of HA-MSA2 conjugate in orthotopic SB28 GBM model

Six-week-old female C57BL/6J mice (Charles River Laboratories, Wilmington, MA, USA) were orthotopically grafted with 5×10^3 cells/mouse by CED. Tumor growth was monitored by IVIS as discussed above. On Day 10, mice were randomized into 3 groups (7 mice/group) and locally treated via CED with MSA2 or HA-MSA2 (5 μg/mouse). Mice without treatment were used as control. Survival study was performed and mice with free access to water and food were monitored daily and were euthanized when reached the following endpoints: (i) 20 % body weight loss or (ii) 10 % body weight loss plus clinical signs of morbidity (e.g., arched back, lack of movement, paralysis). Animal body weight was constantly monitored throughout the experiments.

2.7. Analysis of the local GBM immune microenvironment

Brains were isolated from the animals directly after euthanasia (endpoints). Single-cell suspensions were obtained via mechanical disruption by smashing tissues through a 70 μm cell strainer (Greiner Bio-One, Vilvoord, Belgium), and the cells were counted, washed with PBS and processed. The single-cell suspensions were first incubated for 10 min on ice with TruStain FcX™ blocking solution and then stained with fluorochrome-labeled antibodies and analyzed using an LSR Fortessa flow cytometer (BD Biosciences) and FlowJo software (TreeStar). Intracellular staining was performed by incubating the cells for 30 min at RT in a permeabilization/fixation solution (eBioscience™ Foxp3/Transcription Factor Staining Buffer Set; Thermo Fisher Scientific, Waltham, MA, USA) followed by staining with the remaining labeled antibodies. Details of the antibodies used and the gating strategy are given in the SI (table S2 and figs. S4–S7).

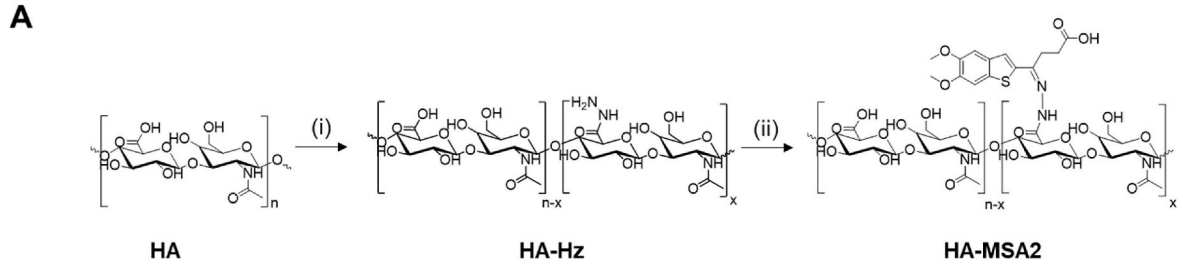

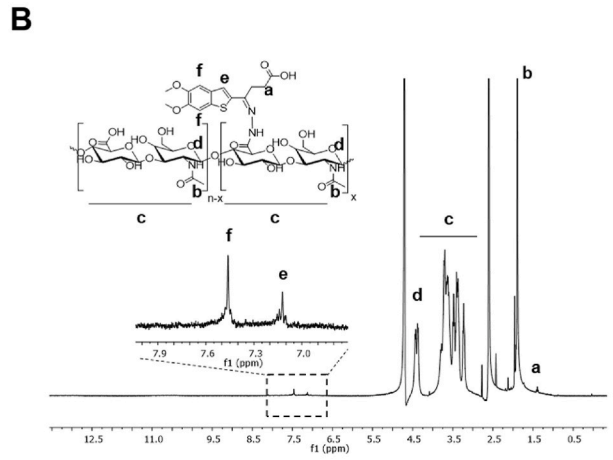

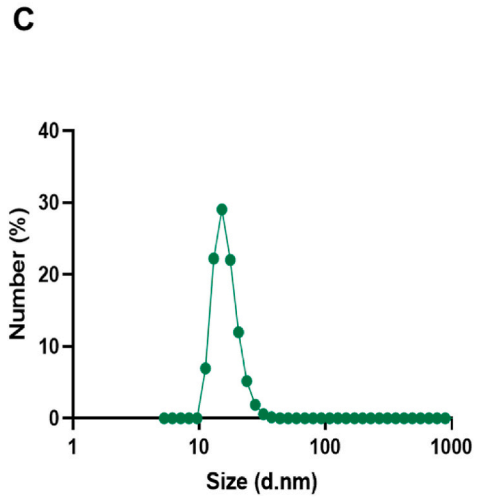

D

Conjugate	HA-MSA2
Drug loading (%w/w)	1.37
Size (nm)	12.96 ± 3.83
Zeta-potential (mV)	-25.78 ± 2.32

Fig. 1. Synthesis and characterization of HA-MSA2 conjugate. A. Synthetic pathway to obtain HA-MSA2; (i) DMTMM Cl, water, room temperature, 96 h and (ii) MSA2 in DMF (5 mg/mL) in water supplemented of 1 % of acetic acid, pH = 5. **B.** ^{1}HNMR of HA-MSA2 and relative peaks; **C.** Size of HA-MSA2 conjugate expressed in number; **D.** Summary table of HA-MSA2 conjugate characterization.

2.8. Statistical analyses

Statistical analyses were performed using the statistical software GraphPad Prism (GraphPad Software Version 9.1.2, San Diego, CA, USA). P values < 0.05 were considered significant. For all analyses and each group, any exclusions were supported by the use of the Grubbs test for outlier detection.

3. Results

3.1. Chemical and Structural characterization of STING-activating HA-MSA2 conjugate

MSA2 was conjugated to HA to obtain HA-MSA2 following the strategy depicted in Fig. 1A [52]. In the first step, HA was derivatized with hydrazine; next, taking advantage of the ketone group in the MSA-2 structure, the drug was conjugated to HA through hydrazone as a pH-sensitive linker. The ^{1}H NMR of HA-MSA2 confirmed the chemical identity of the conjugate. The signature peaks of MSA2 are visible in the aromatic region (7.1–7.8 ppm, letters *e* and *f*, respectively in Fig. 1B) indicating the effective incorporation of the drug into the HA backbone. As its quantification by NMR is not possible because of its low peak signal, the amount of drug incorporated in HA-MSA2 was quantified by UV–Vis, and corresponds to 1.37 % w/w. Next, we evaluated the size and the zeta potential of the conjugate. Native HA is a linear polysaccharide and exists in an extended conformation in an aqueous solution; the conjugation with MSA2 induced shrinkage of the polymer backbone and lead to the formation of nano-aggregates with a size of approx. 13 nm (Fig. 1C). This is in agreement with previous reports [55]. The zeta potential values of the HA-MSA2 conjugate were negative (−25.8 mV) which could be ascribed to the negative charge of the surrounding HA corona. The full characterization of HA-MSA2 is reported in Fig. 1D.

3.2. HA-MSA2 conjugate increases STING activation and downstream gene expression in innate immune cells in vitro

In vitro treatment of JAWSII murine dendritic cells (DCs) for 30 min resulted in significantly greater stimulation of STING signaling (phosphorylation of STING, TBK1 and IRF3) by the HA-MSA2 conjugate than by the free drug (Fig. 2A and B; 20 μM MSA2 equivalent concentration); this was followed by activation-associated degradation of STING by 5h and 24h (fig. S1A). To assess the efficacy of HA-MSA2 in activating the innate immune response, we tested the novel conjugate on JAWSII murine DCs, J774 murine macrophages and BV-2 murine microglial cells for 5 h and 24 h, followed by qPCR for the expression of type I Interferon (IFNβ), the immunostimulatory cytokines TNFα and IL6, and the T cell chemokine CXCL10 [30,56]. These markers serve as quantitative read-outs of STING pathway activation and confirmed the stronger effect of HA-MSA2 at 5 h, an effect that is less pronounced after 24 h treatment (Fig. 2C–E). To note, we incubated cells with HA and the levels of cytokines remained similar to the untreated in all the time points studied and for all the immune cells used in the study. This behavior highlights the role of HA as a nanocarrier that boosts the efficacy of MSA2.

3.3. HA-MSA2 induces immunostimulatory gene expression in GBM cells, without upregulating the T cell inhibitor PD-L1

As GBM cells express STING, we hypothesized that HA-MSA2 could also trigger its signaling in SB28 murine GBM cells [30]. While stimulation with HA-MSA2 did not result in significantly higher phosphorylation of STING, TBK1 and IRF3 as compared to stimulation by MSA2 (fig. S1B), qPCR showed a significant difference in downstream (IFNβ, TNFα, IL-6, CXCL10) gene expression by 24 h (Fig. 3). Indeed, the drug alone showed negligible induction of these genes, highlighting the pivotal effect of HA-conjugation in boosting its efficiency. In SB28, the expression of immunostimulatory markers was lower at the early time point analyzed (5h), while the levels were increased at 24 h (Fig. 3A). This trend is the opposite as observed in GL261 (Fig. 3B). We speculate that the last expression of downstream antitumor effectors on SB28 can be ascribed to a superior immune resistance of these cells compared to GL261 which is recognized to be more immunogenic [54]. Although the expression of innate immunity markers is lower for SB28 at 5 h, in cells treated with HA-MSA2, the levels of IFNβ, TNFα, IL-6 and CXCL10 are approximately 2-fold higher compared to other treatments. As in the case of the innate immune cells tested, the results of GBM cells treated with only HA were similar to untreated cells.

Since it has been demonstrated that the STING pathway increases expression of PD-L1 on several cancers (e.g. melanoma, lung cancer), thereby attenuating the activity of cytotoxic T cells [30], we investigated PD-L1 expression on GBM cells upon treatment with the conjugate. Interestingly, the conjugate did not elicit expression of PD-L1 in SB28 GBM cells at 5 h or 24 h, while MSA2 alone slightly increased PD-L1 at 24 h (Fig. 3). Concerning GL261, HA-MSA2 elicited a superior expression of PDL-1 at 5 h while no difference with the controls was observed at 24 h (Fig. 3B). This would suggest that HA-MSA2 can enable a potent activation of innate immune cytokines/chemokines, without inducing negative regulators of T-cell immune function (such as PD-L1) in the GBM cells studied [57].

3.4. STING-activating HA-MSA2 conjugate triggers GBM immunogenic cell death and immune cell maturation

Having shown the improved STING pathway-activating effect of HA-MSA2 in both innate immune and cancer cells, we next explored its impact on cell viability. The median inhibitory concentration (IC_{50}) dose of HA-MSA2 was approximately 10-fold lower than the IC_{50} dose of unconjugated MSA2 (Fig. 4A and B). However, HA-MSA2 did not impact the cell viability of BV-2 cells (fig. S2). Then, we evaluated whether the new conjugate can promote ICD with 'eat me' signals such as the surface expression of calreticulin (CRT) and adenosine triphosphate (ATP) release [57] on GBM cells. HA-MSA2, but not free MSA2, promoted superior translocation of CRT to cell membranes of treated SB28 cells (Fig. 4C). This was consistent with enhanced ATP release from SB28 cells after 24 h of incubation with HA-MSA2 (Fig. 4D). These *in vitro* data suggest that the conjugation of MSA2 to HA elicits stronger STING activation and ICD in GBM cells.

We further explored if SB28 cells pretreated with HA-MSA2 could induce the maturation of innate immune cells (increased levels of CD86). We induced ICD of SB28 by treating them with HA, MSA2 and HA-MSA2, and incubated immune cells with supernatants from these treated cells for 24 h (Fig. 4E). JAWSII, J774 and BV-2 cells incubated with supernatants from HA-MSA2-treated SB28 showed higher expression of CD86 compared to those incubated with supernatant from untreated SB28 cells (Fig. 4F–H). Compared to the free drug, HA-MSA2-treated SB28 cell supernatants induced higher activation not only of dendritic cells but also of macrophages and microglial cells. No significant differences between untreated cells and HA-treated cells were observed. These results suggest that HA-MSA2 can exert both direct (*cis*) and indirect (*trans*) effects to boost innate immunity, by inducing the expression of cytokines/chemokines, as well as promoting ICD.

3.5. Local treatment with HA-MSA2 inhibits GBM growth and extends survival in the SB28 GBM mouse model

To assess whether the novel polymer-drug conjugate could delay tumor growth, increase survival and impact the TIME, we selected the aggressive and notably cold, non-immunogenic SB28 model as a more challenging syngeneic GBM mouse model [54,58]. Mice were orthotopically grafted with SB28 cells and at Day 10, were treated with free MSA2, HA-MSA2 (drug equivalent dose: 5 μg/mouse) using

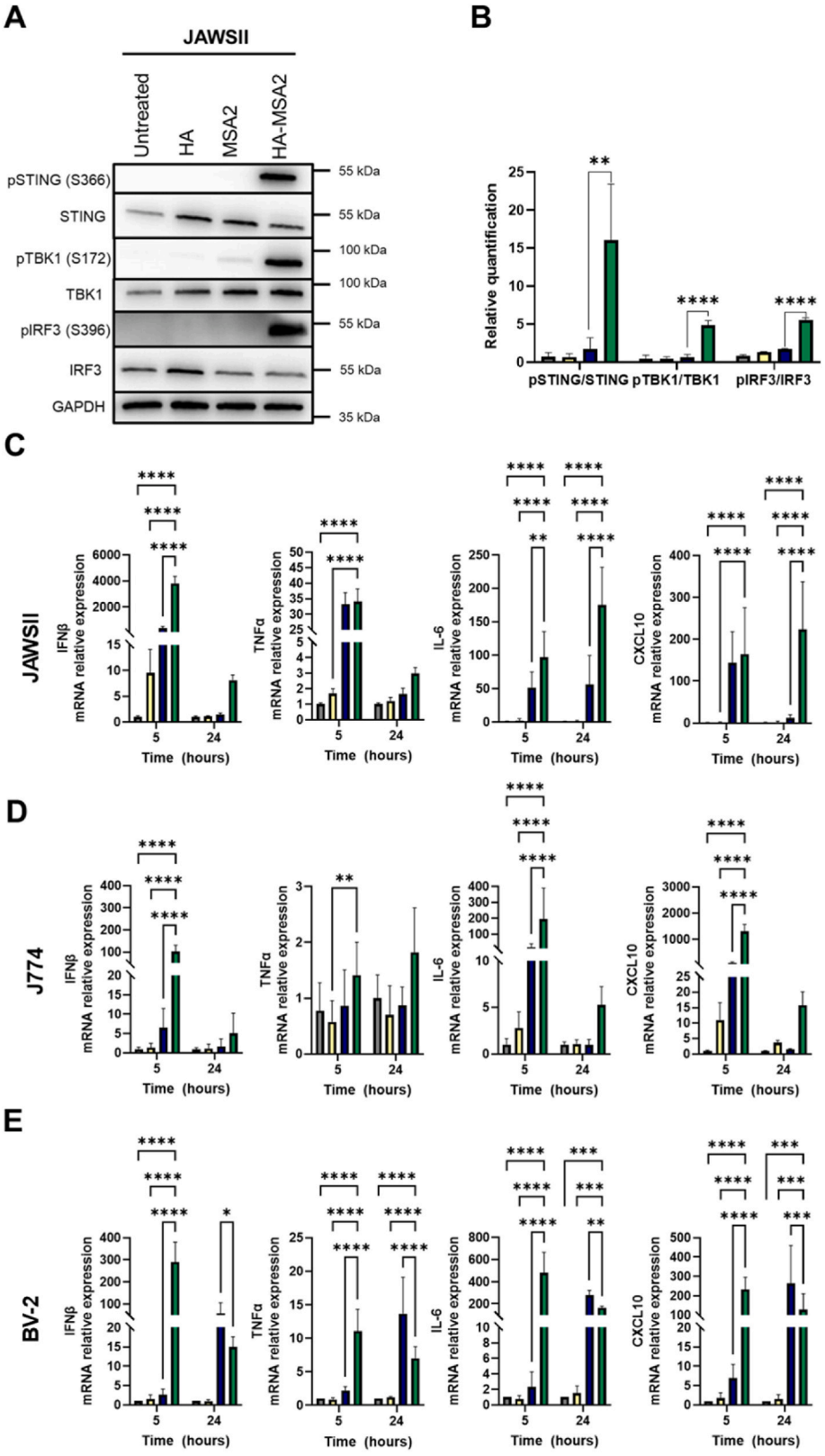

(caption on next page)

Fig. 2. HA-MSA2 activates STING signaling and expression of downstream genes in innate immune cells. A. JAWSII cells were treated with HA, MSA2 or HA-MSA2 (20 μM MSA2 equivalent concentration) for 0.5h; untreated cells were used as controls. Cells were lysed and analyzed by Western blot, using anti-phosphoSTING (p-STING), anti-STING, anti-phospho-TBK1 (*p*-TBK1), anti-TBK1, anti-phopshoIRF3 (pIRF3) and anti-IRF3 antibodies. Anti-GAPDH or anti-alpha actinin were used as loading controls. Representative blots from three replicates; **B.** Blots were quantified, and phospho-protein signal (normalized to GAPDH or alpha actinin on the same blot) was normalized to the corresponding total protein (normalized to GAPDH or alpha actinin on the same blot). Relative quantifications are shown. $^{**}p < 0.01$, $^{****}p < 0.0001$ (One-way ANOVA with Tukey's post-hoc). **C-E.** qPCR gene expression of immune-stimulatory markers (IFNβ, TNFα, IL-6 and CXCL10) after treatment with HA alone, MSA2 or HA-MSA2 of **C.** JAWSII, **D.** J774 and **E.** BV-2 cells for 5 and 24 h. Cells were treated with an equivalent concentration of MSA2 of 20 μM. Untreated cells were used as a reference. Data were normalized to results from untreated cells using RLP19 as a housekeeping gene. Mean, error bar = SD, n = 3, statistical analysis performed via two-way ANOVA followed by Dunnet's multiple comparison test with a single pooled variance ($^{*}p < 0.05$, $^{**}p < 0.01$, $^{***}p < 0.001$, $^{****}p < 0.0001$).

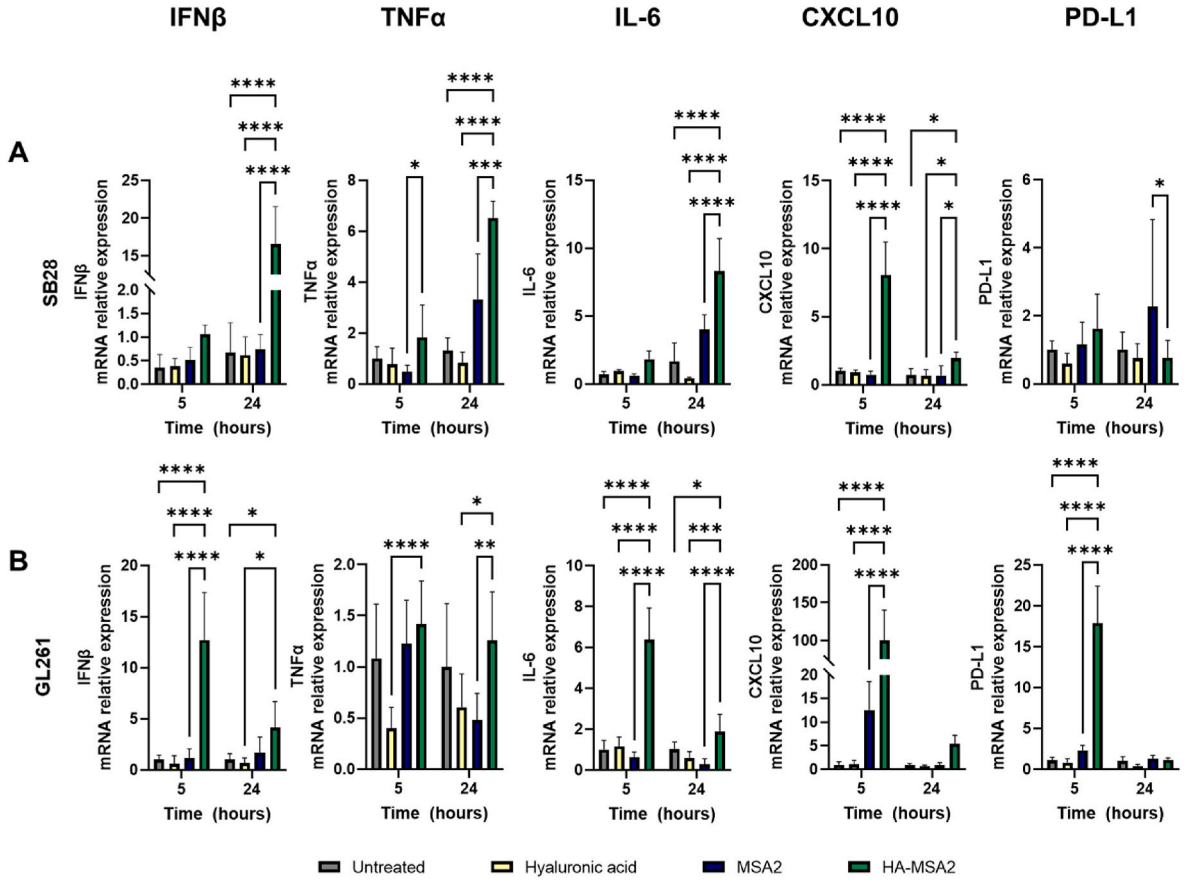

Fig. 3. HA-MSA2 enabled the expression of immunostimulatory gene in GBM cells without the expression of the T cell inhibitor PD-L1. Analysis of immune-stimulatory markers (IFNβ, TNFα, IL-6 and CXCL10) and negative regulators of T cell immune function (PD-L1) by qPCR after treatment with HA alone, MSA2 or HA-MSA2 of **A.** SB28 and **B.** GL261 cells for 5 and 24 h. Cells were treated with an equivalent concentration of MSA2 of 20 μM. Untreated cells were used as a reference. Data were normalized to results from untreated cells using Actin β as a housekeeping gene. Mean, error bar = SD, n = 3, statistical analysis performed via two-way ANOVA followed by Dunnet's multiple comparison test with a single pooled variance ($^{*}p < 0.05$, $^{**}p < 0.01$, $^{***}p < 0.001$, $^{****}p < 0.0001$).

convection-enhanced delivery (CED), or left untreated as reported in Fig. 5A. Mice that received HA-MSA2 showed a delay in tumor growth compared to the other groups (Fig. 5B and C). The dose has been selected considering *a)* toxicity and *b)* solubility issues of free MSA2 (soluble only in DMSO). A slight increase in the bioluminescent tumor-associated signal was observed in the group treated with HA-MSA2 between Days 11 and 14, whereas mice treated with MSA2 showed a luminescence comparable to the untreated group. On Day 14, the HA-MSA2 group showed a reduction of 2.8 times compared to the untreated group. Analysis of tumor size at Day 14 revealed greater uniformity for the group treated with HA-MSA2 compared to the free drug and untreated groups (Fig. 5D). In response to treatment, mice showed a loss in body weight that was transient in the group treated with HA-MSA2 conjugate, but progressive in the MSA2 and untreated groups (Fig. 5E).

The survival analysis reflected the trend observed in the tumor growth curve (Fig. 5F): mice treated with HA-MSA2 (median survival of 25 days) showed a significantly higher median survival compared to the untreated group (19 days). No difference was observed in the median survival of mice treated with the free drug (20 days) compared to the untreated group. These results support the hypothesis that HA is an effective nanocarrier for the *in situ* delivery of therapeutic agents in the context of GBM.

3.6. *In situ administration of HA-MSA2 Drives innate and adaptive immune Cell infiltration and Re-educate GBM TIME*

To obtain a global picture of immune activation following HA-MSA2 treatment of GBM *in vivo*, we performed endpoint analysis of infiltrating innate and adaptive immune cells and the TIME, using a panel of 11 immunological markers in flow cytometry analysis of brain tissue. Our data show that HA-MSA2 induced a complete remodeling of the TIME and its immune composition. Indeed, we observed a significant

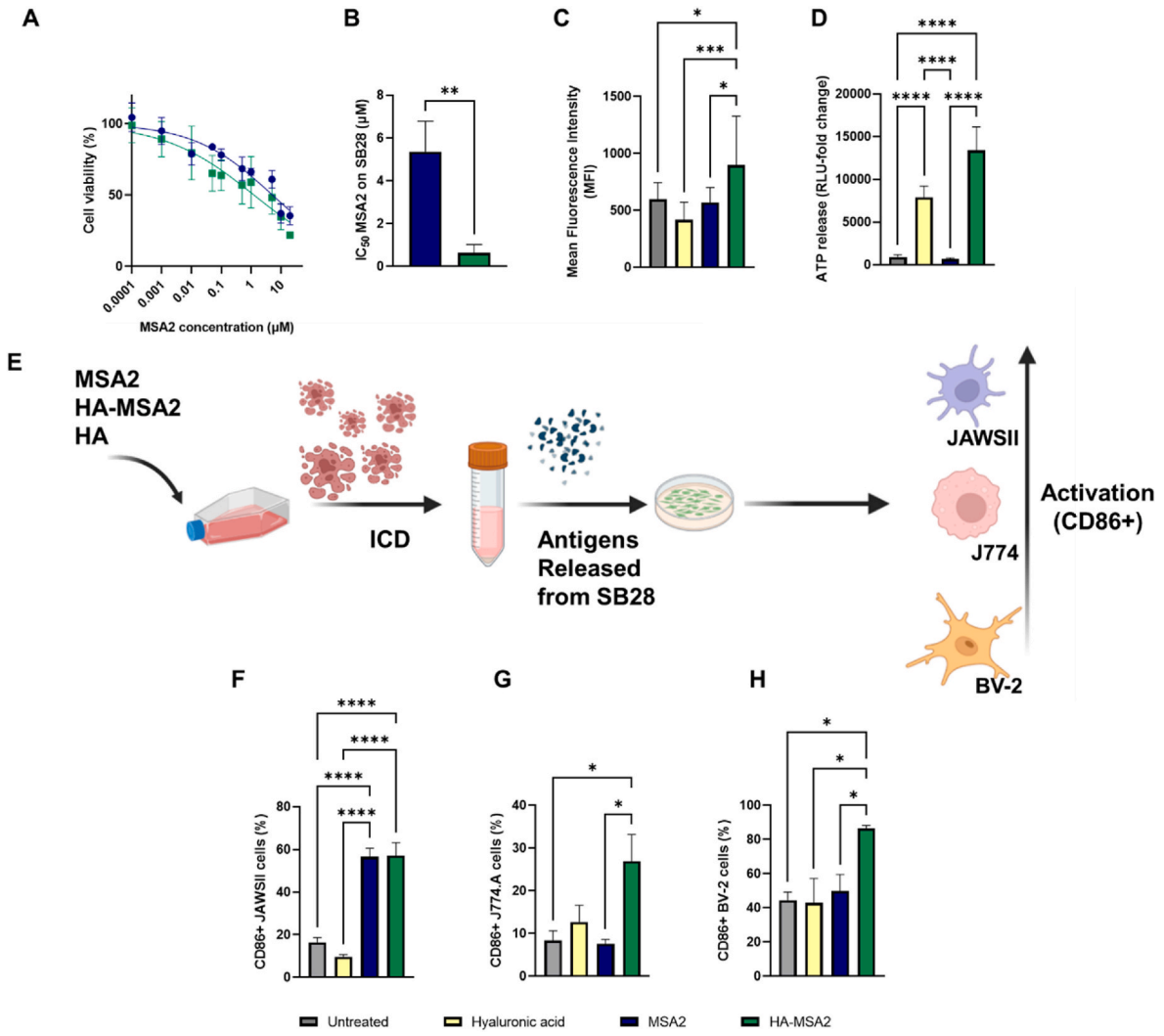

Fig. 4. HA-MSA2 induces cell toxicity in SB28 cells associated with hallmarks of immunogenic cell death and favors the maturation of immune cells. A, B. SB28 cells were treated with MSA2 (blue line) and HA-MSA2 (green line) for 72 h and cell viability was measured; IC_{50} values were obtained by non-linear regression curve fitting; Mean, error bar = SD, n = 3, statistical analysis performed via unpaired *t*-test (**p < 0.01); **C.** Membrane translocation of calreticulin (CRT, calculated as MFI ratio) and **D.** ATP release induced by HA, MSA2 and HA-MSA2. Mean, error bar = SD, n = 3, statistical analysis performed via Kruskal-Wallis test followed by Dunn's multiple comparison test (*p < 0.05, **p < 0.01, ***p < 0.001, ****p < 0.0001). **E.** Schematic representation of immune-cell maturation assay. Percentage of $CD86^+$ **F.** JAWSII, **G.** J774, and **H.** BV-2 cells after incubation with SB28 medium pretreated with HA, MSA2, and HA-MSA2. Mean, error bar = SD, n = 3, statistical analysis performed via One-way ANOVA test followed by Tukey's multiple comparisons test, with a single pooled variance. (*p < 0.05, **p < 0.01, ***p < 0.001, ****p < 0.0001).

activation of the innate immune system, with higher levels of dendritic cells and activated dendritic cells, in mice treated with HA-MSA2 as compared to the MSA2 and untreated groups (Fig. 6A and B). FACS analysis also showed higher frequency of NK cells following treatment with HA-MSA2 (Fig. 6C); no difference in frequency of NK T cells was observed (Fig. 6D). These results highlight the capacity of HA-MSA2 to recruit cells involved in innate immunity in a cold tumor like GBM. Next, we investigated the effect of HA-MSA2 on the frequency of T cells. Brains from HA-MSA2 treated mice had a higher frequency of CD8 T cells and IFNγ-secreting CD8 T cells as compared to the untreated group (Fig. 6E and F). No significant differences were observed for CD4 T cells and IFNγ-secreting CD4 T cells (p = 0.0786) compared to the untreated group (Fig. 6G and H). Moreover, we observed significantly higher levels of expression of perforin, involved in the cytolytic activity of NK and T cells, in the HA-MSA2 group by qPCR (fig. S3). The increase in IL-6 and CCL2 expression, assessed by qPCR, was not significant (fig. S3). Since the efficacy of current immunotherapies is hampered by the presence of Tregs that suppress effector T cells through complex cellular and molecular mechanisms, we analyzed the impact of the conjugate on these immune suppressive cells (Fig. 6I). Although no differences in the frequency of Tregs was observed, the CD8 T cell/Treg ratio increased by 2.17-fold in HA-MSA2-treated versus untreated mice (Fig. 6J). Together, these data suggest that local intratumoral delivery of HA-MSA2 induces more effective remodeling of the TIME and its immune profile, than MSA2 alone.

4. Discussion

The recent discoveries on the role of the STING pathway in cancer immune surveillance, with the possibility of eliciting both innate and adaptive immune responses using the same therapeutic agent, have motivated the study of STING agonists in the context of GBM. Here, we show the efficacy of a novel HA-based conjugate for the local delivery of the STING agonist MSA2, in promoting a potent immune response against GBM. Given the complexity of the GBM TIME, we hypothesized that modulating the activity of the innate and adaptive arms using a polymer-drug conjugate would provide greater therapeutic effects than targeting either arm alone (Fig. 7) [12,33]. We sought to address this

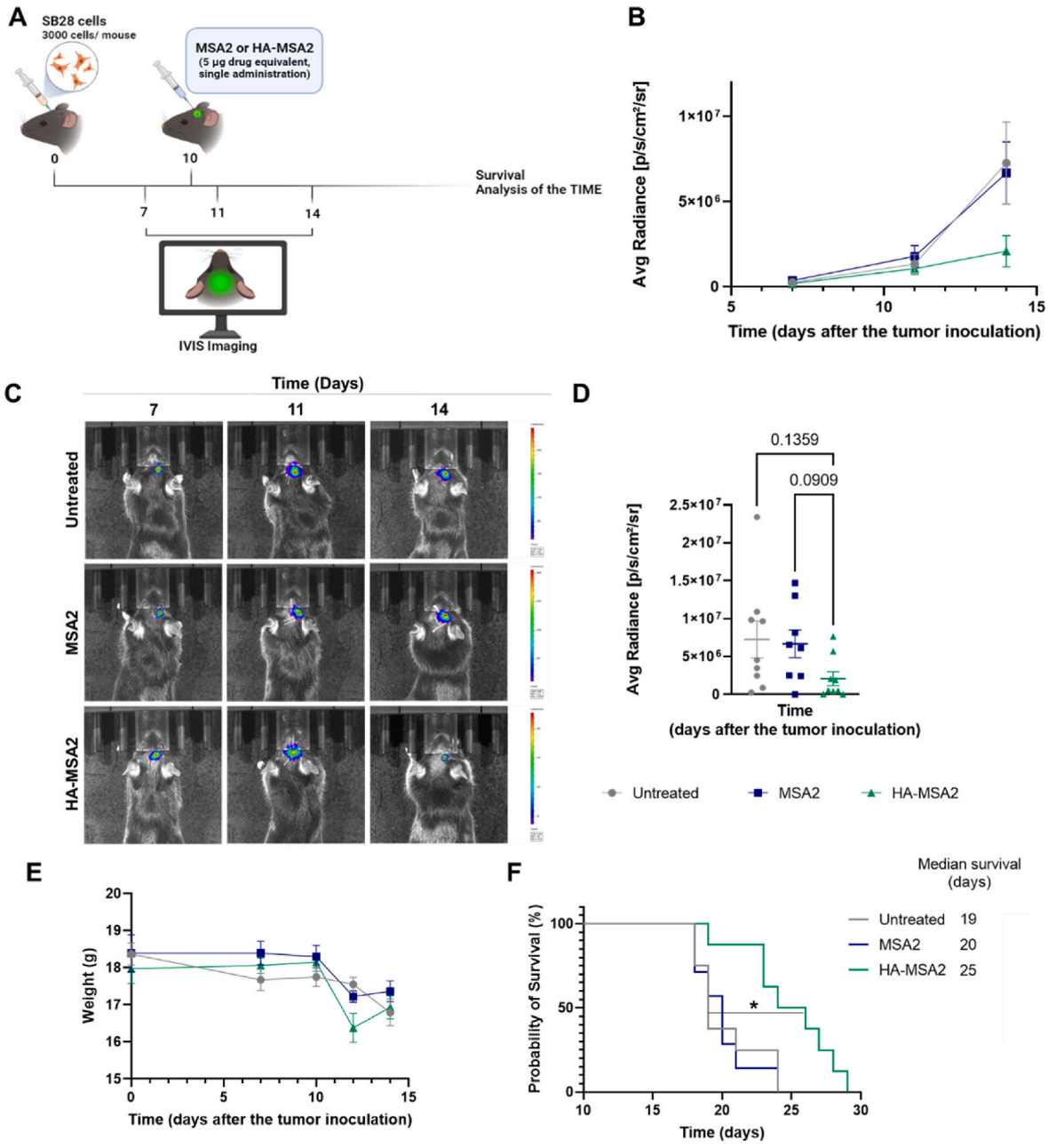

Fig. 5. In situ administration of HA-MSA2 exhibits control of tumor growth and extended survival of SB28-GBM-bearing mice. A. Timeline of the experiment with exact time points for SB28 orthotopically grafting and local treatment. C57BL/6 mice were challenged at Day 0 with 3×10^3 SB28 cells and treated with MSA2 or HA-MSA2 at Day 10 (5 μg MSA2 equivalent dose). Untreated mice did not receive any treatment. Tumor growth was monitored on days 7, 11, and 14 via IVIS imaging. **B, C** Bioluminescent signal associated with GBM growth; **D.** Bioluminescent signal associated with GBM volume at Day 14 post-SB28 tumor induction. Statistical analysis was performed using one-way ANOVA with Dunnett's multiple comparison test; **E.** Bodyweight analysis of mice untreated or treated with MSA2 or HA-MSA2 or left untreated. **F.** Kaplan–Meier survival curves of GBM bearing mice. The error bars represent the mean ± SEM; n = 6–8. Survival curves were analyzed using the Mantel-Cox test (*$p < 0.05$).

challenge by conjugating MSA2 to HA, ameliorating its solubility profile and cell uptake as previously demonstrated with other drugs [59,60]. Compared to our previous approaches [53,61], the advantages reside in a simultaneous trigger of both innate and adaptive immunity with a single immunotherapeutic agent after an intracranial injection.

Leveraging the experience from previously synthesized HA-drug conjugates, we employed a pH-sensitive linker targeting release in endo-lysosomes [52,53]. This approach should ensure effective MSA2 release both in GBM cells and in APCs due to the CD44-mediated cell uptake as demonstrated previously on GBM and microglial cells [52,53]. Importantly, this approach is even more relevant for MSA2, which becomes active after dimerization that occurs at a pH lower than 6.5 [41]. Other conjugation strategies have been explored using the carboxylic acid on MSA2; however, intramolecular cyclization of the drug resulted in conjugation failure (data not shown). Our approach avoids harsh conditions (e.g., high temperature, ultrasound, extreme pH), increasing the feasibility of production in GMP conditions and therefore, clinical translation. We succeeded in conjugating a 1.37 % w/w loading; superior drug loading led to a decrease in water solubility of the conjugate, precluding its use for local treatment of GBM. The process of conjugation also allowed the small MSA2 drug to be converted into a macromolecule with a size of ≈12 nm and a negative zeta potential

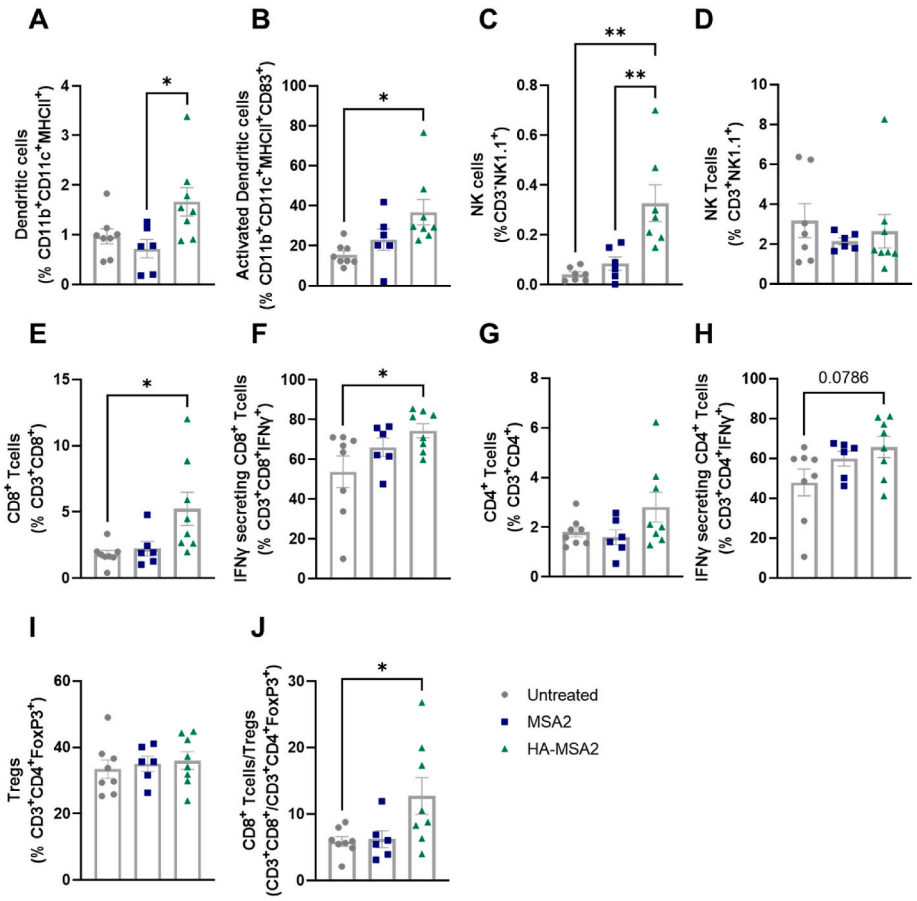

Fig. 6. In vivo immunological effects of local administered HA-MSA2 induce a shift of GBM TIME towards a "hot" phenotype. A. Percent of dendritic cells; **B.** Percent of activated dendritic cells; **C.** Percent of NK cells; **D.** Percent of NK T cells; **E.** Percent of CD8 T cells; **F.** Percent of IFNγ$^+$ CD8 T cells; **G.** Percent of CD4 T cells; **H.** Percent of IFNγ$^+$ CD4 T cells; **I.** Percent of FOXp3$^+$ C T cells (Tregs) and **J.** Ratio between CD8 T cells/Tregs. The error bars represent the mean ± SEM; n = 6–8. Statistical analysis: one-way ANOVA multiple comparison (*p < 0.05, **p < 0.01, ***p < 0.001).

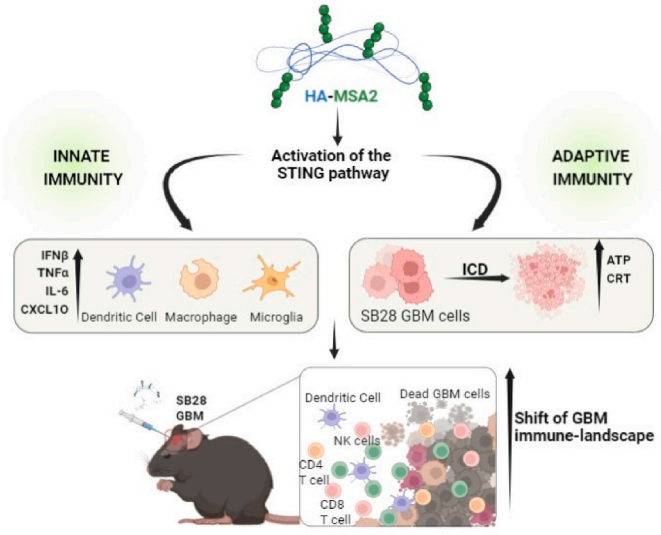

Fig. 7. Graphical schematic of the HA-MSA2 proposed mechanism for anticancer activity. The efficacy of HA-MSA2 lies in its combined stimulation of innate and adaptive immune systems, targeting multiple arms of GBM immunity. HA-MSA2 enables innate immune cell recruitment followed by an increase of CD8 T cells in immunologically "cold" GBM, eliciting a shift in the tumor immune landscape.

(−25 mV). The formation of nanoparticles is in line with previous works [52,53,62]; indeed, the conjugation of hydrophobic drugs such as MSA-2 (computed Log P = 2.3) allows the shrinks of the polymer. GBM possesses a complex architecture with a range of pH, volume of cerebrospinal cord fluid, hypoxia, and mechanical properties (the presence of the extracellular matrix) that vary according to the characteristic and stage of the disease (e.g., dimensions, injuries, anatomical location, etc.). Therefore, it is hard to recapitulate *in vitro* the conditions to evaluate the drug release of MSA-2 from the conjugate, although it is clear that the linking chemistry strongly influences the efficacy, as we previously demonstrated [52].

In vitro studies performed on GBM and immune cells show the capacity of HA-MSA2 to effectively trigger the STING pathway after only 30 min of incubation, and increase downstream gene expression. Conjugating MSA2 to HA increased expression of IFNβ by 8, 16 and 111-fold *in vitro* in DCs, macrophages and microglia cells, respectively, after 5 h of incubation. A similar trend was observed for the other cytokines (TNFα, IL6) and the T cell chemokine (CXCL10) analyzed. While expression of STING-responsive genes was lower in GBM cells as compared to innate immune cells, the HA-conjugate was nevertheless able to induce their expression in the SB28 and GL261 cell lines, in contrast to the unconjugated molecule. We speculate that the efficient triggering of the STING pathway of HA-MSA2 might be ascribed to the structure of the conjugate; indeed, HA-MSA2 can be considered as a "multiple MSA2-prodrug" rather than a conventional drug delivery system. After the cell uptake, HA-MSA2 would provide a superior MSA2 concentration compared to the free drug promoting a faster dimerization and efficacy. Moreover, our data support the hypothesis that HA-

MSA2 can promote an innate immune response via tumor-intrinsic STING activation as well. This corroborates a study that used different polymeric nanoparticles for the delivery of cGAMP to neuroblastoma cells [29,63]. To our knowledge, however, this is the first demonstration of a polymer-STING agonist conjugate eliciting the expression of immunostimulatory genes in "cold" GBM cells themselves.

We observed that HA-MSA2 affects the viability of GBM cells (but not the BV-2 cells), with conjugation reducing the IC_{50} of MSA2 by 10-fold. These results are in agreement with recent findings that demonstrate that the activation of STING can induce cancer cell death [33,53]. HA-MSA2 seems to enable ICD in SB28 cells, which could trigger antitumor innate and adaptive immunity by diverse mechanisms [57]. These results are particularly interesting in the context of GBM, which possesses a low mutational burden and high inter- and intra-patient heterogeneity, hampering the recognition of tumor antigens of anticancer vaccines [12]. These results are even more relevant for SB28 cells where so far only a few hundred antigens have been recognized [54,58]. Our work offers a new strategy to release tumor antigens from cells that are poorly immunogenic but responsive to STING activation. Other groups have shown that delivering STING agonists to cancer cells enhances the efficacy of chemotherapy [64]; Wang-Bishop et al., showed ICD in neuroblastoma cells using cGAMP [33]. However, to the best of our knowledge, this is the first report in which MSA2 has been shown to elicit ICD in GBM.

The promising data from our *in vitro* experiments encouraged us to explore the use of HA-MSA2 in a mouse orthotopic model of GBM. We selected SB28 since it has several characteristics that make it an attractive experimental model to recapitulate human GBM [54]. HA-MSA2 was able to reduce tumor growth over time and improve mice survival compared to the MSA2-treated and untreated groups. Notably, this was achieved using only a single administration of HA-MSA2, with a lower dose compared to other reports for the free drug MSA2 [41]. This highlights the efficacy of our polymer-drug conjugate for stimulating antitumor immunity in GBM.

To understand the effects of HA-MSA2 on the GBM TIME, we characterized the local immune and observed a significant increment of inflammatory cell populations like NK cells, DCs, and T cells. Interestingly, NK cells have been recently highlighted as a major player in STING therapy [65]; although the delay of tumor growth and the extension of survival should be attributed to the cytotoxic effect exerted by CD8 T cells, recent literature suggests the role of NK cells in supporting these cells through direct and indirect pathways [66,67]. This suggests that HA-MSA2 mitigates immunosuppression in the GBM TIME, engaging immunostimulatory mechanisms to enhance T cell infiltration and activity. These results are consistent with a study by Berger et al. showing an increased frequency of pro-inflammatory innate cells post intra-tumoral STING agonist treatment of GBM [30].

Our results support the hypothesis that HA-MSA2 can re-educate the traditional "cold" behavior of GBM by increasing the CD8 T cell/Tregs ratio generating a more inflamed TIME. Overall, these findings demonstrate that HA-MSA2 can trigger a potent immune response against GBM cells, supporting the use of HA as a platform to trigger the immune response of drugs. HA, generally considered a safe biomaterial, may be suitable for clinical translation and quickly locally applied by neurosurgeons. We believe that our approach could be implemented in the future through encapsulation into hydrogels adaptable to fill a tumor-resected cavity, in addition to the standard of care, or in combination with photothermal therapy [68].

5. Conclusions

We introduced a state-of-the-art biodegradable polymer platform to deliver a potent STING agonist MSA2, to simultaneously induce both innate and adaptive immunity for the local treatment of GBM. We demonstrated that the conjugation of MSA2 to HA efficiently triggers the STING pathway and consequently upregulates type I IFN and other cytokines in both immune and GBM cells. Moreover, the novel conjugate induces cytotoxicity in GBM cells via the induction of ICD that can be leveraged to generate anti-GBM immunity. Additionally, STING activation switches highly immunosuppressive GBM to immunogenic TIME, leading to increased DC, NK and CD8 T cell infiltration with an overall induction of antitumor immunity, and extended survival. Our findings support the future exploration of HA-MSA2 as a versatile immunotherapeutic for improving clinical outcomes of other aggressive tumors in combination with various chemo-immunotherapeutics or cancer vaccines.

CRediT authorship contribution statement

Teenesha Chellen: Methodology, Formal analysis, Data curation. **Mathilde Bausart:** Methodology, Investigation, Formal analysis, Data curation. **Pierre Maus:** Methodology, Investigation, Formal analysis. **Kevin Vanvarenberg:** Methodology, Formal analysis. **Nisha Limaye:** Writing – review & editing, Funding acquisition, Data curation. **Véronique Préat:** Writing – review & editing, Supervision, Resources, Project administration, Funding acquisition, Conceptualization. **Alessio Malfanti:** Writing – review & editing, Writing – original draft, Validation, Supervision, Resources, Project administration, Methodology, Investigation, Funding acquisition, Formal analysis, Data curation, Conceptualization.

Declaration of competing interest

The authors declare that they have no known competing financial interests or personal relationships that could have appeared to influence the work reported in this paper.

Data availability

Data will be made available on request.

Acknowledgements

A.M. was supported by the Marie Skłodowska-Curie Actions for an Individual European Fellowship under the European Union's Horizon 2020 research and innovation program (grant agreement no. 887609) and by an FRS-FNRS fellowship (grant agreement no. 40000747) (Belgium). M.B. was supported by a Televie grant. V.P. is supported by Fonds de la Recherche Scientifique—Fonds National de la Recherche Scientifique (FRS-FNRS, grant agreement nos. 33669945, 40003419). P. M. is supported by an F.R.I.A fellowship from the FRS-FNRS. N.L. is a chercheur qualifiée of the FRS-FNRS. N.L. is supported by funds from FRS-FNRS (CDR J.0124.22) and an Actions de Recherche Concertées grant from UCLouvain (A.R.C. grant 19/24-098). We thank Nicolas Dauguet (De Duve Institute, Brussels, Belgium) for the support of flow cytometry analysis. We are grateful to Valentina Marotti (Louvain Drug Research Institute, Brussels, Belgium) for the help in drawing the graphical abstract and Fig. 7.

Appendix A. Supplementary data

Supplementary data to this article can be found online at https://doi.org/10.1016/j.mtbio.2024.101057.

References

[1] C. Bastiancich, P. Danhier, V. Préat, F. Danhier, Anticancer drug-loaded hydrogels as drug delivery systems for the local treatment of glioblastoma, J. Contr. Release 243 (2016) 29–42.

[2] C. Bastiancich, A. Malfanti, V. Préat, R. Rahman, Rationally designed drug delivery systems for the local treatment of resected glioblastoma, Adv. Drug Deliv. Rev. (2021) 113951.

[3] A. Osborn, D. Louis, T. Poussaint, L. Linscott, K. Salzman, The 2021 world health organization classification of tumors of the central nervous system: what neuroradiologists need to know, Am. J. Neuroradiol. 43 (2022) 928–937.

[4] R. Stupp, M. Brada, M. Van Den Bent, J.-C. Tonn, G. Pentheroudakis, High-grade glioma: ESMO Clinical Practice Guidelines for diagnosis, treatment and follow-up, Ann. Oncol. 25 (2014) iii93–iii101.

[5] R. Stupp, W.P. Mason, M.J. Van Den Bent, M. Weller, B. Fisher, M.J. Taphoorn, K. Belanger, A.A. Brandes, C. Marosi, U. Bogdahn, Radiotherapy plus concomitant and adjuvant temozolomide for glioblastoma, N. Engl. J. Med. 352 (2005) 987–996.

[6] R. Stupp, S. Taillibert, A.A. Kanner, S. Kesari, D.M. Steinberg, S.A. Toms, L. P. Taylor, F. Lieberman, A. Silvani, K.L. Fink, Maintenance therapy with tumor-treating fields plus temozolomide vs temozolomide alone for glioblastoma: a randomized clinical trial, JAMA 314 (2015) 2535–2543.

[7] C. Birzu, P. French, M. Caccese, G. Cerretti, A. Idbaih, V. Zagonel, G. Lombardi, Recurrent glioblastoma: from molecular landscape to new treatment perspectives, Cancers 13 (2020) 47.

[8] J.N. Sarkaria, L.S. Hu, I.F. Parney, D.H. Pafundi, D.H. Brinkmann, N.N. Laack, C. Giannini, T.C. Burns, S.H. Kizilbash, J.K. Laramy, Is the blood–brain barrier really disrupted in all glioblastomas? A critical assessment of existing clinical data, Neuro Oncol. 20 (2018) 184–191.

[9] K. Yang, Z. Wu, H. Zhang, N. Zhang, W. Wu, Z. Wang, Z. Dai, X. Zhang, L. Zhang, Y. Peng, Glioma targeted therapy: insight into future of molecular approaches, Mol. Cancer 21 (2022) 1–32.

[10] Z. Xiong, Q. Yang, X. Li, Effect of intra-and inter-tumoral heterogeneity on molecular characteristics of primary IDH-wild type glioblastoma revealed by single-cell analysis, CNS Neurosci. Ther. 26 (2020) 981–989.

[11] P. Johann, D. Lenz, M. Ries, The drug development pipeline for glioblastoma—a cross sectional assessment of the FDA Orphan Drug Product designation database, PLoS One 16 (2021) e0252924.

[12] M. Bausart, V. Préat, A. Malfanti, Immunotherapy for glioblastoma: the promise of combination strategies, J. Exp. Clin. Cancer Res. 41 (2022) 1–22.

[13] M. Bausart, K. Vanvarenberg, B. Ucakar, A. Lopes, G. Vandermeulen, A. Malfanti, V. Préat, Combination of DNA vaccine and immune checkpoint Blockades improves the immune response in an orthotopic Unresectable glioblastoma model, Pharmaceutics 14 (2022) 1025.

[14] A.D. Garg, L. Vandenberk, M. Van Woensel, J. Belmans, M. Schaaf, L. Boon, S. De Vleeschouwer, P. Agostinis, Preclinical efficacy of immune-checkpoint monotherapy does not recapitulate corresponding biomarkers-based clinical predictions in glioblastoma, OncoImmunology 6 (2017) e1295903.

[15] N. Zhang, L. Wei, M. Ye, C. Kang, H. You, Treatment progress of immune checkpoint blockade therapy for glioblastoma, Front. Immunol. 11 (2020) 592612.

[16] K.J. Habashy, R. Mansour, C. Moussalem, R. Sawaya, M.J. Massaad, Challenges in glioblastoma immunotherapy: mechanisms of resistance and therapeutic approaches to overcome them, Br. J. Cancer (2022) 1–12.

[17] M. Jiang, P. Chen, L. Wang, W. Li, B. Chen, Y. Liu, H. Wang, S. Zhao, L. Ye, Y. He, cGAS-STING, an important pathway in cancer immunotherapy, J. Hematol. Oncol. 13 (2020) 1–11.

[18] D. Lee, K. Huntoon, M. Kang, Y. Lu, T. Gallup, W. Jiang, B.Y. Kim, Harnessing cGAS-STING pathway for cancer immunotherapy: from Bench to clinic, Advanced Therapeutics 5 (2022) 2200040.

[19] L.T. Khoo, L.Y. Chen, Role of the cGAS–STING pathway in cancer development and oncotherapeutic approaches, EMBO Rep. 19 (2018) e46935.

[20] B. Hussain, Y. Xie, U. Jabeen, D. Lu, B. Yang, C. Wu, G. Shang, Activation of STING based on its structural Features, Front. Immunol. 13 (2022).

[21] X. An, Y. Zhu, T. Zheng, G. Wang, M. Zhang, J. Li, H. Ji, S. Li, S. Yang, D. Xu, An analysis of the expression and association with immune cell infiltration of the cGAS/STING pathway in pan-cancer, Mol. Ther. Nucleic Acids 14 (2019) 80–89.

[22] Y. Do, P.S. Nagarkatti, M. Nagarkatti, Role of CD44 and hyaluronic acid (HA) in activation of alloreactive and antigen-specific T cells by bone marrow-derived dendritic cells, J. Immunother. 27 (2004) 1–12.

[23] E. Vachon, R. Martin, V. Kwok, V. Cherepanov, C.-W. Chow, C.M. Doerschuk, J. Plumb, S. Grinstein, G.P. Downey, CD44-mediated phagocytosis induces inside-out activation of complement receptor-3 in murine macrophages, Blood, The Journal of the American Society of Hematology 110 (2007) 4492–4502.

[24] T. Matsumoto, S. Imagama, K. Hirano, T. Ohgomori, T. Natori, K. Kobayashi, A. Muramoto, N. Ishiguro, K. Kadomatsu, CD44 expression in astrocytes and microglia is associated with ALS progression in a mouse model, Neurosci. Lett. 520 (2012) 115–120.

[25] S.-R. Woo, M.B. Fuertes, L. Corrales, S. Spranger, M.J. Furdyna, M.Y. Leung, R. Duggan, Y. Wang, G.N. Barber, K.A. Fitzgerald, STING-dependent cytosolic DNA sensing mediates innate immune recognition of immunogenic tumors, Immunity 41 (2014) 830–842.

[26] L. Deng, H. Liang, M. Xu, X. Yang, B. Burnette, A. Arina, X.-D. Li, H. Mauceri, M. Beckett, T. Darga, STING-dependent cytosolic DNA sensing promotes radiation-induced type I interferon-dependent antitumor immunity in immunogenic tumors, Immunity 41 (2014) 843–852.

[27] L. Corrales, L.H. Glickman, S.M. McWhirter, D.B. Kanne, K.E. Sivick, G.E. Katibah, S.-R. Woo, E. Lemmens, T. Banda, J.J. Leong, Direct activation of STING in the tumor microenvironment leads to potent and systemic tumor regression and immunity, Cell Rep. 11 (2015) 1018–1030.

[28] M.F. Gulen, U. Koch, S.M. Haag, F. Schuler, L. Apetoh, A. Villunger, F. Radtke, A. Ablasser, Signalling strength determines proapoptotic functions of STING, Nat. Commun. 8 (2017) 1–10.

[29] D. Shae, K.W. Becker, P. Christov, D.S. Yun, A.K. Lytton-Jean, S. Sevimli, M. Ascano, M. Kelley, D.B. Johnson, J.M. Balko, Endosomolytic polymersomes increase the activity of cyclic dinucleotide STING agonists to enhance cancer immunotherapy, Nat. Nanotechnol. 14 (2019) 269–278.

[30] G. Berger, E.H. Knelson, J.L. Jimenez-Macias, M.O. Nowicki, S. Han, E. Panagioti, P.H. Lizotte, K. Adu-Berchie, A. Stafford, N. Dimitrakakis, STING Activation Promotes Robust Immune Response and NK Cell–Mediated Tumor Regression in Glioblastoma Models, vol. 119, Proceedings of the National Academy of Sciences, 2022 e2111003119.

[31] T. Ohkuri, A. Ghosh, A. Kosaka, J. Zhu, M. Ikeura, M. David, S.C. Watkins, S. N. Sarkar, H. Okada, STING Contributes to Antiglioma immunity via triggering type I IFN signals in the tumor MicroenvironmentSTING-mediated Antiglioma immunity, Cancer Immunol. Res. 2 (2014) 1199–1208.

[32] M.C. Hanson, M.P. Crespo, W. Abraham, K.D. Moynihan, G.L. Szeto, S.H. Chen, M. B. Melo, S. Mueller, D.J. Irvine, Nanoparticulate STING agonists are potent lymph node–targeted vaccine adjuvants, The Journal of clinical investigation 125 (2015) 2532–2546.

[33] L. Wang-Bishop, M. Wehbe, D. Shae, J. James, B.C. Hacker, K. Garland, P. P. Chistov, M. Rafat, J.M. Balko, J.T. Wilson, Potent STING activation stimulates immunogenic cell death to enhance antitumor immunity in neuroblastoma, Journal for immunotherapy of cancer 8 (2020).

[34] E.L. Dane, A. Belessiotis-Richards, C. Backlund, J. Wang, K. Hidaka, L.E. Milling, S. Bhagchandani, M.B. Melo, S. Wu, N. Li, STING agonist delivery by tumour-penetrating PEG-lipid nanodiscs primes robust anticancer immunity, Nat. Mater. 21 (2022) 710–720.

[35] P. Dosta, A.M. Cryer, M.Z. Dion, T. Shiraishi, S.P. Langston, D. Lok, J. Wang, S. Harrison, T. Hatten, M.L. Ganno, Investigation of the enhanced antitumour potency of STING agonist after conjugation to polymer nanoparticles, Nat. Nanotechnol. 18 (2023) 1351–1363.

[36] X. Chen, Z. Xu, T. Li, A. Thakur, Y. Wen, K. Zhang, Y. Liu, Q. Liang, W. Liu, J.-J. Qin, Nanomaterial-encapsulated STING agonists for immune modulation in cancer therapy, Biomark. Res. 12 (2024) 2.

[37] L. Zhang, K. Shang, X. Li, M. Shen, S. Lu, D. Tang, H. Han, Y. Yu, Reduction sensitive polymers delivering Cationic platinum drugs as STING agonists for enhanced chemo-immunotherapy, Adv. Funct. Mater. 32 (2022) 2204589.

[38] M. Shen, Y. Wang, T. Bing, Y. Tang, X. Liu, Y. Yu, Alendronate triggered Dual-cascade targeting prodrug nanoparticles for enhanced tumor Penetration and STING activation of Osteosarcoma, Adv. Funct. Mater. 33 (2023) 2307013.

[39] S.-J. Zheng, M. Yang, J.-Q. Luo, R. Liu, J. Song, Y. Chen, J.-Z. Du, Manganese-based immunostimulatory metal–organic framework activates the cGAS-STING pathway for cancer Metalloimmunotherapy, ACS Nano 17 (2023) 15905–15917.

[40] J. Liu, X. Huang, J. Ding, Identification of MSA-2: an oral antitumor non-nucleotide STING agonist, Signal Transduct. Targeted Ther. 6 (2021) 1–2.

[41] B.-S. Pan, S.A. Perera, J.A. Piesvaux, J.P. Presland, G.K. Schroeder, J.N. Cumming, B.W. Trotter, M.D. Altman, A.V. Buevich, B. Cash, An orally available non-nucleotide STING agonist with antitumor activity, Science 369 (2020) eaba6098.

[42] M. Yi, M. Niu, Y. Wu, H. Ge, D. Jiao, S. Zhu, J. Zhang, Y. Yan, P. Zhou, Q. Chu, Combination of oral STING agonist MSA-2 and anti-TGF-β/PD-L1 bispecific antibody YM101: a novel immune cocktail therapy for non-inflamed tumors, J. Hematol. Oncol. 15 (2022) 1–21.

[43] M. Wehbe, L. Wang-Bishop, K.W. Becker, D. Shae, J.J. Baljon, X. He, P. Christov, K. L. Boyd, J.M. Balko, J.T. Wilson, Nanoparticle delivery improves the pharmacokinetic properties of cyclic dinucleotide STING agonists to open a therapeutic window for intravenous administration, J. Contr. Release 330 (2021) 1118–1129.

[44] M.B. Ashford, R.M. England, N. Akhtar, Highway to success—developing advanced polymer therapeutics, Adv. Therap. 4 (2021) 2000285.

[45] D. Jiang, J. Liang, P.W. Noble, Hyaluronan as an immune regulator in human diseases, Physiol. Rev. 91 (2011) 221–264.

[46] D. Si, F. Yin, J. Peng, G. Zhang, High expression of CD44 predicts a poor prognosis in glioblastomas, Cancer Manag. Res. 12 (2020) 769.

[47] R. Prevo, S. Banerji, D.J. Ferguson, S. Clasper, D.G. Jackson, Mouse LYVE-1 is an endocytic receptor for hyaluronan in lymphatic endothelium, J. Biol. Chem. 276 (2001) 19420–19430.

[48] M.E. Mummert, Immunologic roles of hyaluronan, Immunol. Res. 31 (2005) 189–205.

[49] B.-L. Sun, L.-h. Wang, T. Yang, J.-y. Sun, L.-l. Mao, M.-f. Yang, H. Yuan, R. A. Colvin, X.-y. Yang, Lymphatic drainage system of the brain: a novel target for intervention of neurological diseases, Progress in neurobiology 163 (2018) 118–143.

[50] S.S. Chandran, D. Verhoeven, J.R. Teijaro, M.J. Fenton, D.L. Farber, TLR2 engagement on dendritic cells promotes high frequency effector and memory CD4 T cell responses, J. Immunol. 183 (2009) 7832–7841.

[51] S.S. Lee-Sayer, Y. Dong, A.A. Arif, M. Olsson, K.L. Brown, P. Johnson, The where, when, how, and why of hyaluronan binding by immune cells, Front. Immunol. 6 (2015) 150.

[52] A. Malfanti, G. Catania, Q. Degros, M. Wang, M. Bausart, V. Préat, Design of Bio-responsive hyaluronic acid–doxorubicin conjugates for the local treatment of glioblastoma, Pharmaceutics 14 (2022) 124.

[53] G. Catania, G. Rodella, K. Vanvarenberg, V. Préat, A. Malfanti, Combination of hyaluronic acid conjugates with immunogenic cell death inducer and CpG for glioblastoma local chemo-immunotherapy elicits an immune response and induces long-term survival, Biomaterials (2023) 122006.

[54] V. Genoud, E. Marinari, S.I. Nikolaev, J.C. Castle, V. Bukur, P.-Y. Dietrich, H. Okada, P.R. Walker, Responsiveness to anti-PD-1 and anti-CTLA-4 immune checkpoint blockade in SB28 and GL261 mouse glioma models, OncoImmunology 7 (2018) e1501137.

[55] V. Krishnan, K. Peng, A. Sarode, S. Prakash, Z. Zhao, S.K. Filippov, K. Todorova, B. R. Sell, O. Lujano, S. Bakre, Hyaluronic acid conjugates for topical treatment of skin cancer lesions, Sci. Adv. 7 (2021) eabe6627.
[56] R. Falahat, A. Berglund, R.M. Putney, P. Perez-Villarroel, S. Aoyama, S. Pilon-Thomas, G.N. Barber, J.J. Mulé, Epigenetic Reprogramming of Tumor Cell–Intrinsic STING Function Sculpts Antigenicity and T Cell Recognition of Melanoma, vol. 118, Proceedings of the National Academy of Sciences, 2021 e2013598118.
[57] L. Galluzzi, A. Buqué, O. Kepp, L. Zitvogel, G. Kroemer, Immunogenic cell death in cancer and infectious disease, Nat. Rev. Immunol. 17 (2017) 97–111.
[58] A.F. Haddad, J.S. Young, D. Amara, M.S. Berger, D.R. Raleigh, M.K. Aghi, N. A. Butowski, Mouse models of glioblastoma for the evaluation of novel therapeutic strategies, Neuro-oncology advances 3 (2021) vdab100.
[59] C.-P. Fu, X.-Y. Cai, S.-L. Chen, H.-W. Yu, Y. Fang, X.-C. Feng, L.-M. Zhang, C.-Y. Li, Hyaluronic acid-based nanocarriers for anticancer drug delivery, Polymers 15 (2023) 2317.
[60] N.G. Kotla, I.L. Mohd Isa, A. Larrañaga, B. Maddiboyina, S.K. Swamy, G. Sivaraman, P.K. Vemula, Hyaluronic acid-based Bioconjugate systems, Scaffolds, and their therapeutic potential, Adv. Healthcare Mater. 12 (2023) 2203104.
[61] M. Bausart, G. Rodella, M. Dumont, B. Ucakar, K. Vanvarenberg, A. Malfanti, V. Préat, Combination of local immunogenic cell death-inducing chemotherapy and DNA vaccine increases the survival of glioblastoma-bearing mice, Nanomed. Nanotechnol. Biol. Med. 50 (2023) 102681.
[62] D.R. Vogus, M.A. Evans, A. Pusuluri, A. Barajas, M. Zhang, V. Krishnan, M. Nowak, S. Menegatti, M.E. Helgeson, T.M. Squires, A hyaluronic acid conjugate engineered to synergistically and sequentially deliver gemcitabine and doxorubicin to treat triple negative breast cancer, J. Contr. Release 267 (2017) 191–202.
[63] L. Wang-Bishop, B.R. Kimmel, V.M. Ngwa, M.Z. Madden, J.J. Baljon, D.C. Florian, A. Hanna, L.E. Pastora, T.L. Sheehy, A.J. Kwiatkowski, STING-activating nanoparticles normalize the vascular-immune interface to potentiate cancer immunotherapy, Science Immunology 8 (2023) eadd1153.
[64] S. Chattopadhyay, Y.-H. Liu, Z.-S. Fang, C.-L. Lin, J.-C. Lin, B.-Y. Yao, C.-M.J. Hu, Synthetic immunogenic cell death mediated by intracellular delivery of STING agonist nanoshells enhances anticancer chemo-immunotherapy, Nano Lett. 20 (2020) 2246–2256.
[65] C.J. Nicolai, N. Wolf, I.-C. Chang, G. Kirn, A. Marcus, C.O. Ndubaku, S. M. McWhirter, D.H. Raulet, NK cells mediate clearance of CD8+ T cell–resistant tumors in response to STING agonists, Science immunology 5 (2020) eaaz2738.
[66] O. Demaria, A. De Gassart, S. Coso, N. Gestermann, J. Di Domizio, L. Flatz, O. Gaide, O. Michielin, P. Hwu, T.V. Petrova, STING activation of tumor endothelial cells initiates spontaneous and therapeutic antitumor immunity, Proc. Natl. Acad. Sci. USA 112 (2015) 15408–15413.
[67] N.R. Mahadevan, E.H. Knelson, J.O. Wolff, A. Vajdi, M. Saigí, M. Campisi, D. Hong, T.C. Thai, B. Piel, S. Han, Intrinsic immunogenicity of small cell lung carcinoma revealed by its cellular plasticity, Cancer Discov. 11 (2021) 1952–1969.
[68] M. Sun, Y. Li, W. Zhang, X. Gu, R. Wen, K. Zhang, J. Mao, C. Huang, X. Zhang, M. Nie, Allomelanin-based biomimetic nanotherapeutics for orthotopic glioblastoma targeted photothermal immunotherapy, Acta Biomater. 166 (2023) 552–566.